Development 140, 2734-2745 (2013) doi:10.1242/dev.097618

Laminin β1a controls distinct steps during the establishment of digestive organ laterality

Tatiana Hochgreb-Hägele[1,2,*,¶], Chunyue Yin[1,‡,*], Daniel E. S. Koo[2], Marianne E. Bronner[2] and Didier Y. R. Stainier[1,§,¶]

SUMMARY

Visceral organs, including the liver and pancreas, adopt asymmetric positions to ensure proper function. Yet the molecular and cellular mechanisms controlling organ laterality are not well understood. We identified a mutation affecting zebrafish laminin β1a (*lamb1a*) that disrupts left-right asymmetry of the liver and pancreas. In these mutants, the liver spans the midline and the ventral pancreatic bud remains split into bilateral structures. We show that *lamb1a* regulates asymmetric left-right gene expression in the lateral plate mesoderm (LPM). In particular, *lamb1a* functions in Kupffer's vesicle (KV), a ciliated organ analogous to the mouse node, to control the length and function of the KV cilia. Later during gut-looping stages, dynamic expression of Lamb1a is required for the bilayered organization and asymmetric migration of the LPM. Loss of Lamb1a function also results in aberrant protrusion of LPM cells into the gut. Collectively, our results provide cellular and molecular mechanisms by which extracellular matrix proteins regulate left-right organ morphogenesis.

KEY WORDS: Asymmetry, Laminin, Organogenesis

INTRODUCTION

Rather than displaying bilateral symmetry, most non-paired and visceral organs, such as the heart, liver and pancreas, reside on a particular side of the midline. Establishment of left-right (L-R) asymmetry is an important aspect of organogenesis and involves a sequence of molecular and morphogenetic events. L-R asymmetry initiates at gastrula stages via activity of motile cilia in the organizer/node, or Kupffer's vesicle (KV) in zebrafish (Capdevila et al., 2000; Levin, 2005), and its maintenance depends on the integrity of midline structures such as the notochord. Organ chirality ultimately emerges as the morphological outcome of this sequence of signaling cues (Danos and Yost, 1996; Ryan et al., 1998; Bisgrove et al., 2000; Chin et al., 2000; Horne-Badovinac et al., 2003; Long et al., 2003). Disruption of these events results in congenital conditions such as *situs inversus* and heterotaxy.

Fluid flow generated by nodal ciliary movements initiates L-R asymmetry (Nonaka et al., 1998) that is transferred to the lateral plate mesoderm (LPM), as revealed by Nodal expression in the left LPM (Levin et al., 1995; Collignon et al., 1996; Lowe et al., 1996; Lustig et al., 1996; Long et al., 2003). Expression of the Nodal-related gene *southpaw* (Long et al., 2003), and of the Nodal-induced genes *pitx2* (Logan et al., 1998; Piedra et al., 1998; Ryan et al., 1998; Yoshioka et al., 1998; Campione et al., 1999; Essner et al., 2000) and *lefty1* (Meno et al., 1996; Bisgrove et al., 1999; Branford et al., 2000), is restricted to the left LPM. The notochord not only serves as a midline physical barrier (Danos and Yost, 1996), but also plays an active role in the consolidation of the asymmetric expression of Nodal in the LPM via midline expression of the inhibitor factor Lefty (Nakamura et al., 2006; Tabin, 2006), thereby ensuring organ chirality.

The downstream cellular mechanisms underlying asymmetric organ morphogenesis take place substantially later in development. In amniotes, expression of *Pitx2* is restricted to the left dorsal mesentery that connects the midgut to the body wall (Danos and Yost, 1996; Hecksher-Sørensen et al., 2004; Davis et al., 2008; Kurpios et al., 2008), where it locally translates the L-R signals into the differential cellular organization between the left and right LPM, resulting in leftward tilting of the gut tube. Similarly, in zebrafish, asymmetric migration of the LPM displaces the underlying gut endoderm to adopt an asymmetric configuration (Horne-Badovinac et al., 2003). Little is known about the effector mechanisms ultimately connecting early asymmetric signals with later tissue morphogenesis.

There is increasing evidence supporting the importance of the extracellular matrix (ECM) during the establishment of L-R asymmetry. For example, disruption of integrinα5β1 or fibronectin during gastrulation affects the development of the node/KV in zebrafish and *Xenopus*, resulting in defective L-R asymmetry (Ablooglu et al., 2010; Pulina et al., 2011). Studies in mouse and *Xenopus* have shown that proteoglycans facilitate and provide directional cues for rapid propagation of Nodal and Lefty signaling from the node to the left LPM (Oki et al., 2007), and subsequently from the left to the right LPM (Oki et al., 2007; Marjoram and Wright, 2011). ECM proteins also play crucial roles in downstream morphogenetic events underlying organ asymmetry. *In silico* analysis of the formation of gut asymmetry in amniotes predicts that a synergy between epithelial cell-cell adhesion and ECM deposition between left and right sides leads to asymmetric cell compaction and movement in the dorsal mesentery (Kurpios et al., 2008). In zebrafish, the LPM cells degrade the basement membrane at the LPM-gut boundary. Such LPM-ECM interaction is necessary for

[1]Department of Biochemistry and Biophysics, Programs in Developmental and Stem Cell Biology, Genetics and Human Genetics, Liver Center and Diabetes Center, Institute for Regeneration Medicine, University of California, San Francisco, CA 94158, USA. [2]Division of Biology, California Institute of Technology, Pasadena, CA 91125, USA.

*These authors contributed equally to this work
‡Present address: Division of Gastroenterology, Hepatology and Nutrition, Cincinnati Children's Hospital Medical Center, Cincinnati, OH 45229, USA
§Present address: Department of Developmental Genetics, Max Planck Institute for Heart and Lung Research, Bad Nauheim, Hessen D-61231, Germany
¶Authors for correspondence (hochgreb@caltech.edu; didier.stainier@mpi-bn.mpg.de)

Accepted 22 April 2013

the asymmetric migration of the LPM and gut-looping morphogenesis (Yin et al., 2010).

Here, we report that laminin plays an essential role in the establishment of L-R asymmetry of the zebrafish liver and pancreas. Laminins are large heterotrimeric glycoproteins, comprising of α, β and γ chains assembled into a cross-shaped molecule with a long arm and three short globular arms (Engel et al., 1981; Miner, 2008). We present a novel mutant allele of the laminin β1a (*lamb1a*) gene, which encodes a subunit of the ECM protein laminin 1. In this mutant, the liver spans the midline, and the ventral pancreatic bud remains split into bilateral structures. We find that laminin is necessary for controlling cilia length and fluid flow in the KV, and for restricting *southpaw* expression to the left LPM. Subsequently, *lamb1a* deficiency disrupts the dynamic deposition of laminin 1 in the LPM epithelium, resulting in a severely disorganized epithelium with abnormal protrusions into the gut, and a failure of asymmetric gut looping. Thus, laminin 1 participates in sequential events that are important for the establishment of L-R asymmetry of visceral organs, including an early role in the KV and a later role in the LPM.

MATERIALS AND METHODS

Animals

Adult fish and embryos were maintained as described previously (Westerfield, 1995). We used the following lines: *Tg(XlEef1a:GFP)*^{s854} (Field et al., 2003) and *Tg(hand2:EGFP)*^{pd24} (Kikuchi et al., 2011). The *grumpy/lamβ1*^{m189} mutant line (Parsons et al., 2002) was used to test complementation. The *lamb1a*^{s804} mutant was identified in an ENU mutagenesis screen (Ober et al., 2006).

Cloning and genotyping of *lamb1a*^{s804}

Mapping showed that the *s804* mutation was on LG25 near *lamb1a*. The known *lamb1a* mutant allele *grumpy*^{m189} failed to complement the *s804* allele. The *lamb1a* gene was amplified by PCR for sequencing: block A (5′-GTTACAACTCGCAGCCCTTT-3′, 5′-ACTTGGCTTCCTCTGCTTCA-3′), block B (5′-TACCGGAAGGAACTGTGACC-3′, 5′-GCCGTAATAGCCAAGTCTGC-3′), block C (5′-TTTTGTGTCTGCAACCAAGG-3′, 5′-GCGCTGATAATCTCCAGGTC-3′) and block D (5′-TGGCTGGACAGCTAGAGACA-3′, 5′-TGTGCTGTAGACGGTCACTTT-3′). We PCR amplified each block from cDNAs obtained from pooled *s804* mutant embryos, or from their wild-type/heterozygous siblings.

The alternative splice variants of *lamb1a* generated by the *s804* mutation were detected by PCR amplification of Block C. Identity of different splice variants was confirmed by direct sequencing.

A G-to-T mutation in the splice donor site of exon 24 of *lamb1a* was identified in *s804* mutant embryos, resulting in the loss of a *Sna*BI restriction site. Embryos were genotyped by PCR-RFLP: a 286 bp genomic region spanning exons 24-25 is PCR-amplified (5′-CGAAAACAGTGCCAACTCAA-3′, 5′-TGAGCGACTTCAGTTTGGTG-3′), and subsequent digestion with *Sna*BI produces two bands in wild type (93 bp and 193 bp), while the mutant fragment (286 bp) is not cleaved.

Morpholino injections

Single-cell embryos were injected with 3.8 ng of *lamb1a* splice-blocking morpholino (*lamb1a* MO: 5′-TAAATCCGTTGACTGCTTTACCTTC-3′) or 2 ng of *ntl* or *flh* morpholino (Nasevicius and Ekker, 2000; Clanton et al., 2013) in Tris (pH 8.0) and Phenol Red. For midblastula stage injections, *lamb1a* MO was co-injected with 1:1000 rhodamine dextran as a tracer into the yolk of *Tg(XlEef1a:GFP)*^{s854} embryos at 3 hpf (Amack and Yost, 2004). Embryos were sorted at 6-8 hpf for homogeneous distribution of rhodamine throughout the yolk, and analyzed at 52 hpf. Although MO injections at the one-cell stage recapitulated the *lamb1a*^{s804} mutant phenotypes, such as shortened tail and flattened somites, injections at 3 hpf did not cause obvious body phenotypes (data not shown).

In situ hybridization and immunohistochemistry

Whole-mount *in situ* hybridization was performed as described previously (Thisse et al., 1993) using probes for *southpaw*/*spaw* (Long et al., 2003), *no tail* (Schulte-Merker et al., 1992), *foxa3* (Chen et al., 2001), *myl7* (Yelon et al., 1999) and *insulin* (Biemar et al., 2001).

Immunohistochemistry was performed on 150 μm vibratome sections as described (Trinh and Stainier, 2004; Yin et al., 2010). Embryos were fixed in 4% paraformaldehyde in PBS and embedded in 4% low-melting agarose in PBS. Antibodies used were: chick anti-GFP (Aves Labs) at 1:1000, mouse anti-ZO-1 (Invitrogen) at 1:200, mouse anti-islet 1 (Developmental Studies Hybridoma Bank) at 1:10, rabbit anti-laminin (Sigma) at 1:100, rabbit anti-pan-cadherin (Sigma) at 1:100, mouse anti-acetylated tubulin (Sigma) at 1:500 and phalloidin (Molecular Probes) at 1:100. Sections were imaged on a Zeiss Pascal confocal microscope.

Cilia measurements

Embryos fixed at 7-8 ss were immunostained for acetylated tubulin, laminin 1 and phalloidin, mounted in agarose for confocal imaging using an LSM510 inverted confocal microscope, and subsequently genotyped by PCR-RFLP. Cilia length was measured as the distance between two points intersected with a specific channel for acetylated tubulin using the 'Measurement Points' tool in Imaris software (Bitplane).

Analysis of LPM migration

Expression of *Tg(hand2:EGFP)* in the LPM of wild-type and *lamb1a*^{s804} mutant embryos was used to examine the time-course of LPM migration. Embryos were fixed at 1-hour intervals between 25 and 30 hpf, immunostained for GFP and phalloidin, and vibratome-sectioned for confocal imaging.

Analysis of KV flow

Embryos at 6-8 ss were mounted in agarose and injected into the KV (Yuan et al., 2013) with ~1.5 nl of deep red PS-Speck fluorescent beads (Invitrogen) diluted in Ringer's solution. Mounted embryos were imaged with an LSM510 inverted confocal scope at maximum speed over 5 minutes (1000 frames). Quantification of the fluid flow was performed by analysis using the Particle Tracking tools in Imaris software.

Statistical analysis

Differences in the numbers of *Tg(hand2:EGFP)*-expressing cells and non-expressing cells in the LPM of wild-type and mutant embryos were analyzed by the Student's *t*-test (Fig. 5I). Analysis of differences in the distribution of phenotypes between mutants/morphants and controls was performed by the contingency table χ^2 statistical test.

RESULTS

Characterization of *s804* mutants

The *s804* mutant was identified in a forward genetic screen using *Tg(XlEef1a:GFP)*^{s854}, a transgenic zebrafish line expressing green fluorescent protein (GFP) throughout the developing endoderm (Field et al., 2003; Ober et al., 2006). The mutant exhibits lateral expansion of the visceral organ region and loss of asymmetric L-R positioning of the pancreas and liver. At 30 hours post fertilization (hpf), using expression of *Tg(Xla.Eef1a1:GFP)* and the gut marker *foxa3* to label the entire gut primordium (Chen et al., 2001), we observed that the gut loops to the left in wild-type embryos (95%, *n*=71/75) (Fig. 1A,B), but stays in the midline in *s804* mutants (76%, *n*=37/49) (Fig. 1A′,B′). Although animals with impaired gut laterality often exhibit defects in cardiac asymmetry (Danos and Yost, 1996; Ryan et al., 1998; Bisgrove et al., 2000; Chin et al., 2000; Horne-Badovinac et al., 2003; Long et al., 2003), over 85% of *s804* mutants examined showed normal cardiac asymmetry at 35 hpf, as revealed by the left-sided expression of the cardiomyocyte marker *myl7* (Fig. 1B,B′,C) (Yelon et al., 1999). At 72 hpf, the liver and pancreas are situated on the left and right sides of wild-type larvae, respectively (92%, *n*=57/62) (Fig. 1D). In *s804* mutants, however, the ventral pancreatic bud splits into bilateral organs (71%, *n*=26/37) and the liver spans the midline (79%, *n*=29/37) (Fig. 1D′) (*P*<0.001). Although we occasionally observed inversion of visceral

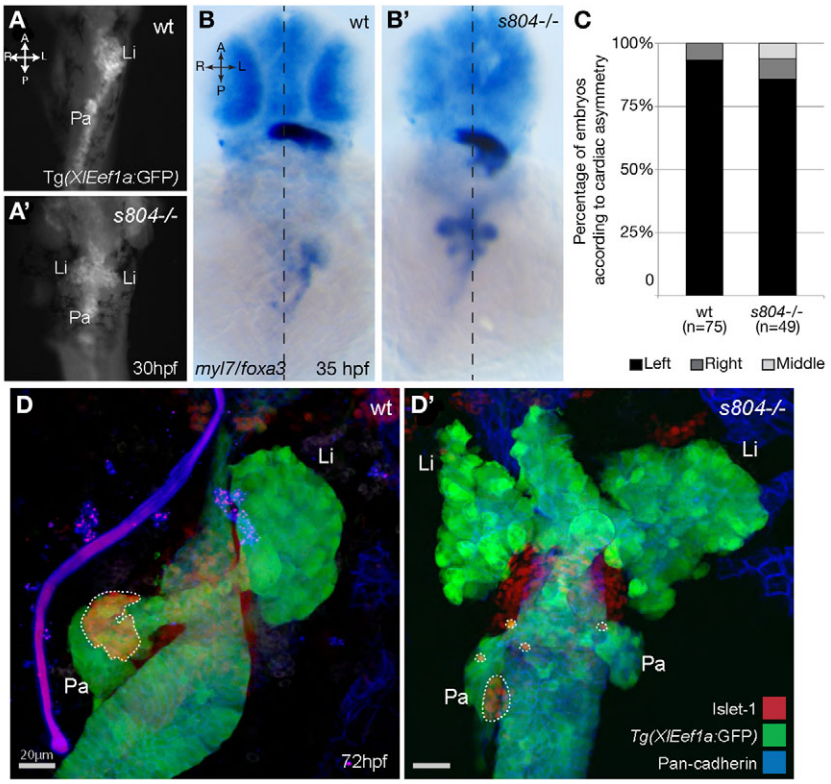

Fig. 1. *s804* mutants display defects in left-right asymmetry of endodermal organs. (**A**,**A′**) The liver (Li) and pancreas (Pa) in wild-type and *s804* mutants are revealed by GFP expression in the enhancer trap line *Tg(XlEef1a:GFP)*. Ventral views, anterior towards the top. (**B**,**B′**) *myl7* and *foxa3* expression in wild-type (B) and *s804* mutants (B′), as revealed by whole-mount *in situ* hybridization. *myl7* is expressed in cardiomyocytes and *foxa3* is expressed in the gut primordium. Dorsal views. Dashed lines mark the midline. (**C**) Repartition of embryos according to cardiac asymmetry, as determined by *myl7* expression. The numbers of embryos analyzed are indicated at the bottom. (**D**,**D′**) Confocal imaging projection of the liver (Li) and pancreas (Pa) at 72 hpf in wild-type (D) and *s804* mutants (D′), as revealed by *Tg(XlEef1a:GFP)* expression (green). Ventral views. Islet 1 (red); pan-cadherin (blue). Dotted lines outline islet1-positive endocrine cells in the principal islet and throughout the hepatopancreatic ductal system. Scale bars: 20 μm.

organ sidedness (n=3/62) in wild-type embryos, we never found this phenotype in *s804* mutants.

To further assess endodermal organ development in *s804* mutants, we examined the expression of various endodermal marker genes. In zebrafish, endodermal progenitors are specified around the margin at the late blastula stage (Stainier, 2002) and undergo convergent extension movements to form a sparse monolayer along the anteroposterior axis, then moving medially to form a solid multicellular rod at the midline by 20 hpf. This endodermal rod forms the endodermal components of the alimentary canal and its connected organs, including the liver and pancreas (Field et al., 2003). Early endodermal morphogenesis appears unaffected in *s804* mutants, as assessed by *sox17* (Alexander and Stainier, 1999) and *foxa1* (Ober et al., 2003) expression; *s804* mutants form an endodermal rod by 20 hpf (data not shown). The endocrine pancreas and liver are properly specified in the mutants by 26 hpf (not shown), with normal *insulin* (Argenton et al., 1999; Biemar et al., 2001) and *hhex* (Ho et al., 1999; Ober et al., 2006) expression. However, expression of islet 1 and insulin proteins at 72 hpf revealed isolated pancreatic endocrine cells that failed to home to the principal islet and were instead randomly dispersed within the hepatopancreatic ductal system (Fig. 1D′).

Cloning of the *s804* mutation

s804 mutants present a shortened body phenotype, similar to other *laminin*-deficient mutants (Parsons et al., 2002). Genetic mapping placed the *s804* mutation on linkage group 25, which contains the genes encoding Lamb1a and Lamb4. Moreover, we found that the *s804* mutation failed to complement the *grumpy/lamb1a*$^{m189-/-}$ allele (Parsons et al., 2002).

We thus cloned *lamb1a* from a pool of *s804* mutant embryos, or their wild-type and heterozygous siblings (Fig. 2A). The *s804* mutant carries a G-to-T point mutation that disrupts the splice donor site (bold, AC**G**T) of exon 24 of the *lamb1a* gene (Fig. 2B), producing alternative splice variants (Fig. 2C) and a frame-shift causing loss of the coiled-coil domains that are necessary for assembly of the trimeric laminin 1 protein. PCR amplification of Block C from wild-type cDNA produces a band of 1.54 kilobases (kb) (Fig. 2A,D). The *s804* mutation predominantly causes aberrant excision of exon 24, resulting in a loss of 370 bp in the transcript sequence (Fig. 2C,D). A second variant results from persistence of intron 24 (+0.9 kb). Interestingly, splicing of exon 23 into a cryptic splice acceptor site within exon 24 (score 0.69, http://www.fruitfly.org/seq_tools/splice.html) produces a third band of 1.3 kb. When Block C was amplified from cDNA obtained from a pool of phenotypically normal embryos (*s804* +/+ and +/−), the 1.54 kb fragment was the most abundant PCR product (Fig. 2D). Traces of alternative size bands were not detected in *grumpy/lamb1a*^{m189} mutant or wild-type embryos, suggesting that these bands were due to the mixed nature of the *s804* sample rather than to naturally occurring splicing variants. Finally, injection of a splice blocking morpholino (MO) designed against the junction of exon 26-intron 26 recapitulated the *s804* mutant phenotype (Fig. 2E).

Laminin protein expression is impaired in multiple tissues in *lamb1a*^{s804} mutants

Laminins are an integral part of the scaffolding of basement membranes. Lam1 is formed by the specific assembly of the α1, β1 and γ1 chains at the coiled-coil long arm (Beck et al., 1990). In zebrafish, Lam1 is localized to the basement membranes associated with the neural tube, notochord, somites and skin at 16 ss (Fig. 2F,G). At 30 hpf, Lam1 is also expressed in the basement membrane of the dorsal aspect of the LPM (Fig. 2H, arrows) and at the boundary between the LPM and gut endoderm (Fig. 2H, arrowheads) (Yin et al., 2010).

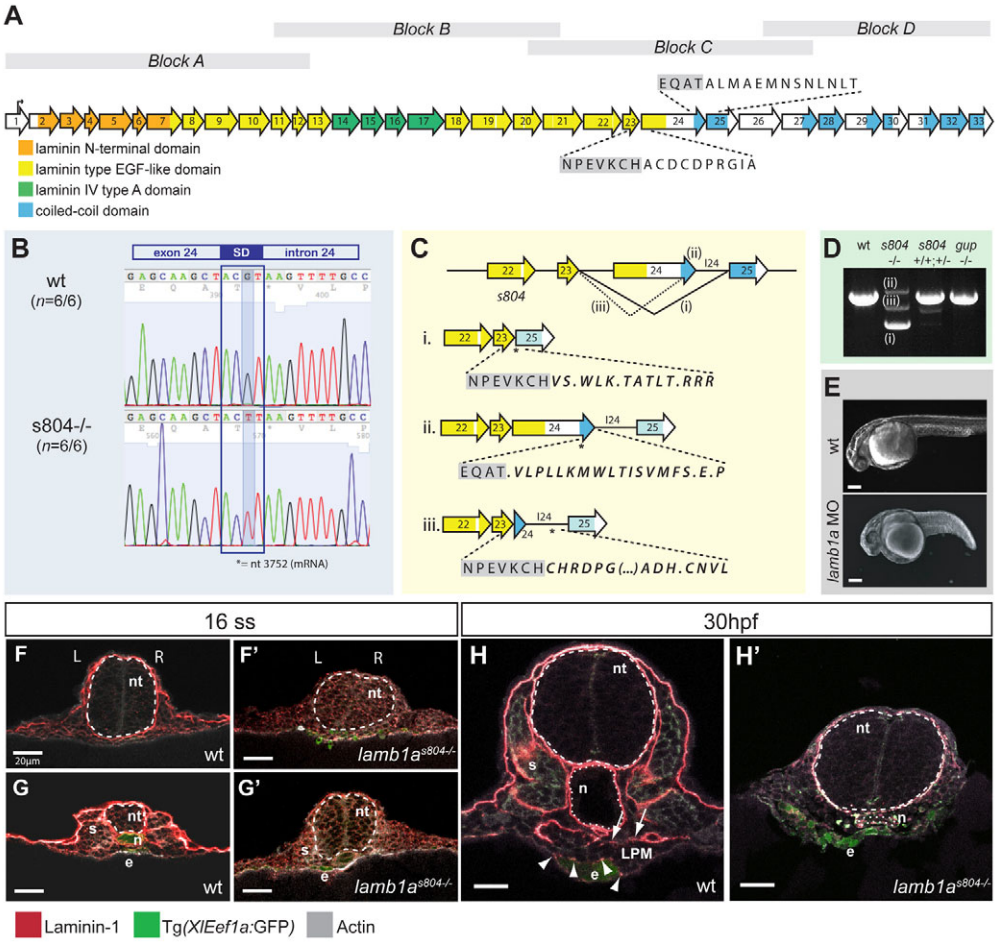

Fig. 2. Mutation in a splice donor (SD) site of the *lamb1a* gene results in a truncated protein in *s804* mutants and impairs expression of the multimeric protein laminin 1 in the basement membrane of *lamb1a*^{s804} mutants. (**A**) The *lamb1a* ORF in zebrafish (exons are numbered). Functional domains of the corresponding protein are represented by colored boxes. Gray blocks represent the cloning strategy. (**B**) G-to-T replacement in the SD site for exon 24 of *lamb1a* in *s804* mutants (6/6). (**C**) Alternative splicing in *lamb1a*^{s804} mutants. Mutation of the SD site for exon 24 results in excision of exon 24 (i), maintenance of intron 24 (I24, ii) or splicing of exon 23 into a cryptic site within exon 24 (iii). These alternative splice events result in a frame-shift and premature stop signals (asterisks) that disrupt the C-terminal coiled-coil domains (blue boxes). (**D**) PCR amplification of block C from wild-type cDNA produces a single band of 1.5 kb. In *s804* mutants, alternative products are detected. (**E**) Injection of a *lamb1a* splice-blocking MO recapitulates the *s804* mutant phenotype. Scale bars: 20 μm. (**F-H'**) Transverse sections of wild-type (F,G,H) and *lamb1a*^{s804} mutant (F′,G′,H′) embryos at 16 ss (F-G′) and 30 hpf (H,H′). Anterior (F,F′) and posterior (G,G′) level sections. Lam1 (red), *Tg(XIEef1a:GFP)* (green). L, left; R, right. Scale bars: 20 μm. Neural tube (nt, broken line), notochord (n), somite (s) and gut endoderm (e). Dotted line identifies marked atrophy of the notochord.

In *lamb1a*^{s804} mutants, Lam1 deposition was greatly reduced (Fig. 2F′,G′), with only patches of residual expression around the neural tube and vestigial notochord at 30 hpf (Fig. 2H′). The diffuse signal seen by immunodetection of Lam1 in *lamb1a*^{s804} mutants may result from the failure of laminin monomers to assemble in the absence of the coiled-coil domain of the β1 subunit, which causes them to accumulate intracellularly.

lamb1a^{s804} mutants exhibit defects in both the notochord and KV cilia

The striking organ laterality defects observed in *lamb1a*^{s804} mutants prompted us to investigate whether the expression of L-R genes was impaired in these embryos. We examined the expression of the Nodal-related factor gene *southpaw* (*spaw*), one of the early factors in the gene cascade involved in the establishment of L-R asymmetry (Long et al., 2003). In wild-type embryos, expression of *spaw* is restricted to the left LPM at 21 ss. However, in *lamb1a*^{s804} mutants, *spaw* is expressed bilaterally (70.5%, *n*=12/17), suggesting that Lamb1a is required for restriction of *spaw* expression to the left LPM (Fig. 3A,B).

Establishment of L-R gene expression depends on the integrity of the KV cilia and notochord: whereas ciliary movements in the KV contribute to the initial establishment of asymmetry, midline structures function as a chemical and/or physical barrier between the right and left sides of the embryo (Danos and Yost, 1996; Meno et al., 1998; Nakamura et al., 2006). Analysis of Lam1 deposition during the stages of KV morphogenesis (Oteíza et al., 2008) shows that Lam1 is detected as scattered puncta associated with epiblast cell membranes during gastrulation (Fig. 3E) (Latimer and Jessen, 2010). Concurrently, a fibrillar assembly of Lam1 is also observed in the mesendoderm-yolk boundary near the embryonic margin (Fig. 3F). From the 1 ss, strong homogeneous expression of Lam1 is detected in the chordamesoderm and in the basement membrane of the ectoderm. In the KV, however, discrete foci of Lam1

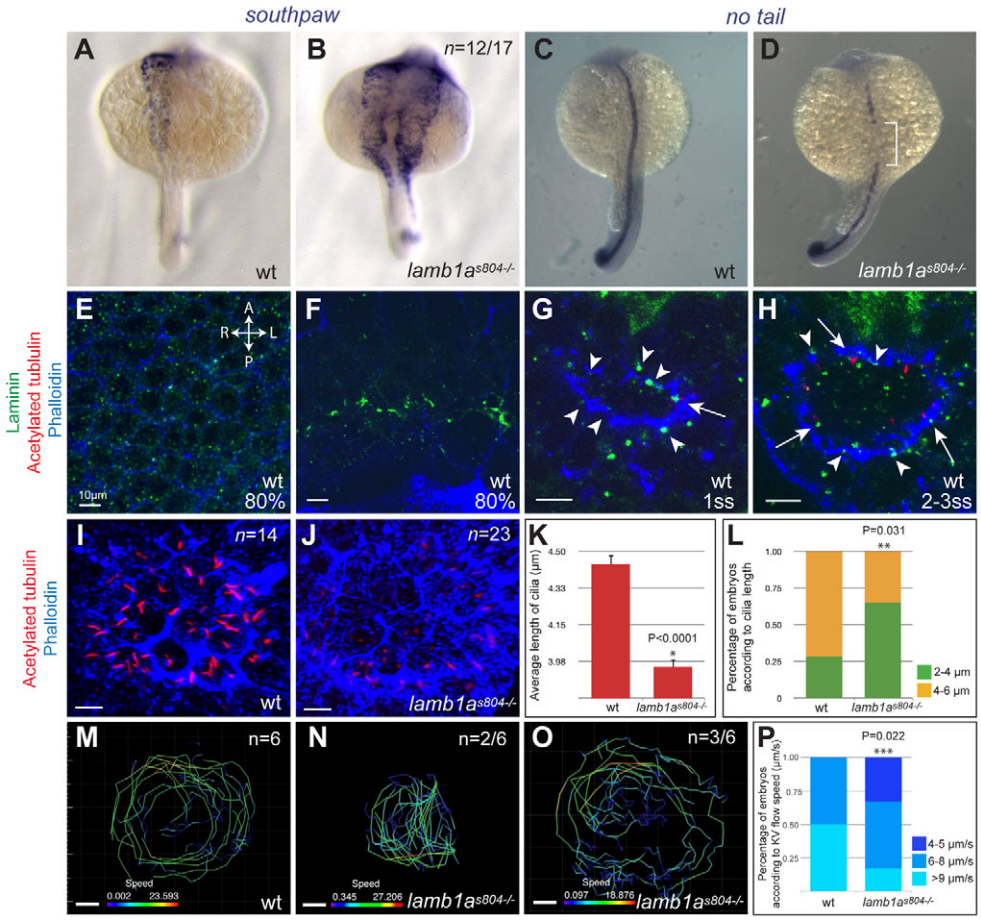

Fig. 3. Lamb1a plays multiple roles in the establishment of left-right asymmetry. (**A**,**B**) Establishment of L-R gene expression machinery is examined by expression of *southpaw/spaw* in wild-type (A) and *lamb1a*^{s804} mutant (B) embryos at 21 ss. (**C**,**D**) Integrity of the notochord is assessed by expression of *no tail/ntl* at 21 ss. Reduction of *ntl* expression in *lamb1a*^{s804} mutants is restricted to the level of the visceral organ-forming region (white bracket). (A-D) Dorsal views. (**E-H**) Single-plane confocal imaging of wild-type embryos stained for Lam1 (green), acetylated tubulin (red) and phalloidin (blue). Dorsal views, anterior towards the top. Expression of Lam1 during KV morphogenesis in the epiblast (E) and at the margin (F) of 80% epiboly stage embryos. Discrete foci of Lam1 deposition are associated with the lumen of the vesicle (G, arrowheads) and where cilia formation takes place (H, arrows). Scale bars: 10 µm. (**I**,**J**) Confocal imaging projection of KV cilia at 8 ss, as revealed by acetylated tubulin staining (red) in wild-type (I) and *lamb1a*^{s804} mutant (J) embryos. Counterstaining by phalloidin (blue). Scale bars: 10 µm. Dorsal views, anterior towards the top. (**K**,**L**) Quantitative analysis (mean±s.e.m.) of KV cilia length in wild type and *lamb1a*^{s804} mutants. Asterisks indicate statistical significance, **P*<0.0001 and ***P*=0.031. (**M-O**) Projection of bead trajectories depicts the fluid flow in the KV of wild-type (M) and *lamb1a*^{s804} mutant (N,O) embryos at 10-12 ss. Lines depicting trajectories of beads within the KV and speed (µm/s) shown are for a representative embryo. (**P**) Quantitative analysis (mean±s.e.m.) of KV fluid flow in wild-type and *lamb1a*^{s804} mutant embryos. Results depict average KV flow speed in six wild-type and six *lamb1a*^{s804} mutant embryos. Asterisks indicates statistical significance, ****P*=0.022.

deposition are generally associated with the lumen of the vesicle, at the junctions between cells (Fig. 3G). Interestingly, at 2-3 ss, the cilia tend to localize at the intercellular junctions where Lam1 deposition is detected (Fig. 3H).

As Lam1 is expressed in both the notochord and KV, we asked whether development of either tissue was impaired in *s804* mutants and perhaps contributed to the bilateral expression of *spaw*. To investigate notochord formation in *lamb1a*^{s804} mutants, we examined the expression of *no tail* (*ntl*), a marker expressed along the entire axial mesoderm of wild-type embryos at 21 ss (Fig. 3C) (Halpern et al., 1993; Schulte-Merker et al., 1994). In *lamb1a*^{s804} mutants, *ntl is* specifically downregulated in the trunk region, at the level where the digestive organs develop during subsequent stages (Fig. 3D). Interestingly, expression of *ntl* near the heart-forming region, as well as in the tail region does not appear to be affected in the mutants (Fig. 3C,D). These findings are consistent with the intact cardiac asymmetry in these embryos, thus suggesting that regulation of L-R asymmetry of the heart versus gut looping is uncoupled in *lamb1a*^{s804} mutants.

To examine KV cilia in *lamβ1*^{s804} mutants, we performed immunostaining using an anti-acetylated tubulin antibody in embryos at 7-8 ss (Piperno and Fuller, 1985; Essner et al., 2005) (Fig. 3I,J). Cilia length was significantly reduced in *lamb1a*^{s804} mutants, with an average±s.e.m. of 3.95±0.09 µm (*n*=23 embryos, 1179 cilia) in contrast to 4.44±0.11 µm in wild-type siblings (*n*=14, 830 cilia) (*P*<0.0001) (Fig. 3K). The shortened cilia length in *lamb1a*^{s804} mutants is associated with a shift in the distribution of cilia length (*P*=0.031). For each embryo, the cilia were classified according to their length. At 8 ss, 71.4% of the wild-type embryos contained KV cilia that were predominantly 4-6 µm long (10/14 embryos), followed by a second class of embryos (28.6%) with predominance of cilia length in the range of 2-4 µm. By contrast,

cilia length was predominantly shorter (2-4 μm) in 65% of the *lamb1a*^{s804} mutants examined (*n*=15/23), with the other 35% of the embryos (*n*=8/23) showing cilia length mainly in the range of 4-6 μm (Fig. 3L). Overall cilia number was not significantly affected in *lamb1a*^{s804} mutants (data not shown).

To determine whether this difference in the KV cilia length affected their function in *lamb1a*^{s804} mutants, we examined the generation of fluid flow in the KV of wild-type and mutant embryos. Analysis of the dynamics of fluorescent beads injected into the KV at 8-10 ss showed that deficiency in Lamb1a expression did not halt fluid flow in the KV and that directionality was also largely preserved in the mutants (data not shown). Instead, we observed variable defects in the size of the KV and the speed of flow in the mutants (Fig. 3M-P). In all the mutants, tracking of the beads showed more erratic trajectories and increased tendency to cross the center of the vesicle (Fig. 3N), in contrast to the regular pattern of fluid flow in the KV of wild-type embryos, where the beads mostly concentrated in the periphery of the vesicle (*n*=5/6) (Fig. 3M). In 50% of the *lamb1a*^{s804} mutant embryos analyzed (*n*=3/6), the KV appeared smaller, yet the average flow speed (7.99±0.13 μm/s) was not significantly affected, when compared with the average traveling speed of 7.65±0.11 μm/s (average±s.e.m.) measured in wild-type and heterozygous embryos (*n*=6). In one-third of the mutants analyzed (*n*=2/6), whereas the KV size was normal, the speed of fluid flow was reduced, with an average speed of 4.58±0.11 μm/s (Fig. 3O). Overall, our analysis of the KV fluid flow indicates that the average flow speed in wild-type embryos ranges between 6 and 10 μm/s (*n*=6). By contrast, in *lamb1a*^{s804} mutant embryos, we observed increased prevalence of embryos with reduced flow (average speed of 4-5 μm/s) (*P*=0.02) (Fig. 3P).

Taken together, our analyses suggest that loss of Lamβ1 function in *lamb1a*^{s804} mutants impairs the integrity of the KV cilia and notochord, both of which are essential for L-R gene expression.

Knockdown of *lamb1a* in the KV causes randomization of gut L-R asymmetry

Given that *lamba1*^{s804} mutants show defects in both the notochord and KV, we examined which defect directly accounted for impaired L-R patterning. To test the role of Lamb1a in the KV, we injected the *lamb1a* MO into the yolk of embryos at midblastula stages to specifically target the dorsal forerunner cells that will form the KV (Amack and Yost, 2004) (Fig. 4A).

We assessed the morphology of the digestive organs based on *Tg(XlEef1a:GFP)* expression at 52 hpf (Fig. 4B-E). Embryos injected with control MO displayed a normal gut phenotype, with the liver and pancreas located on the left and right sides of the embryo, respectively, and the gut displaying an S-shape curvature (85.7%, *n*=36/42). By contrast, only 47.6% (*n*=20/42) of embryos injected with *lamb1a* MO showed a similar leftward gut looping, and 28.6% of the *lamb1a* MO-injected embryos exhibited bilateral liver and pancreas accompanied by the absence of gut looping (*n*=12/42) when compared with 4.8% (*n*=2/42) of the control MO-injected embryos. In addition, we observed an increased occurrence of inverted liver and pancreas position in *lamb1a* MO-injected embryos (23.8%, *n*=10/42), compared with 9.5% in the control MO group (*n*=4/42) (*P*=0.001) (Fig. 4F). Injections of *lamb1a* MO after

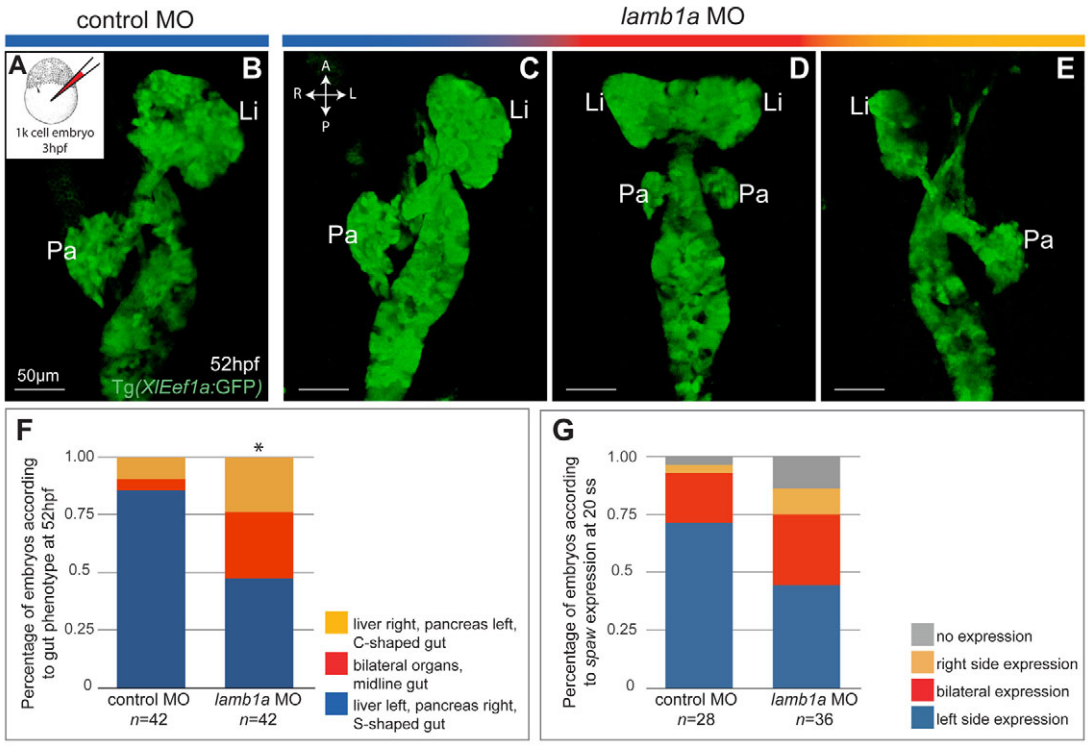

Fig. 4. Knockdown of *lamb1a* in the KV results in randomization of liver and pancreas asymmetry. (**A-E**) Confocal imaging of the gut in *Tg(XlEef1a:GFP)* embryos injected at 3 hpf (A) with control (B) or *lamb1a* (C-E) MO. Effect of KV knockdown of *lamb1a* on the L-R asymmetry of the liver (Li) and pancreas (Pa) was analyzed at 52 hpf. Resulting phenotypes of the liver and pancreas after KV-specific *lamb1a* knockdown include: wild type (C, blue); bilateral liver and pancreas and midline gut (D, red); inversion of L-R asymmetry, with the liver and pancreas localized to the right and left sides of the embryo, respectively (E, yellow). Ventral views. (**F**) Percentages (mean±s.e.m.) of embryos displaying distinct liver and pancreas L-R asymmetry phenotypes. Forty-two embryos were analyzed for each treatment. Asterisks indicate statistical significance, **P*=0.001. (**G**) Percentages (mean±s.e.m.) of embryos showing distinct *spaw* expression patterns at 20 ss. Wild-type embryos were injected with control (*n*=28) or *lamb1a* (*n*=36) MO at 3 hpf.

midblastula stages did not significantly affect L-R asymmetry of the liver and pancreas.

Knocking down *lamb1a* in the KV led to randomization of the gut laterality, rather than failure of gut looping, as in most *lamb1a*^{s804} mutants. Whereas the majority of *lamb1a*^{s804} mutants showed bilateral *spaw* expression during somitogenesis (Fig. 3B), sidedness of *spaw* expression after *lamb1a* knockdown in the KV was rather random, with 44% of the embryos showing normal left-sided *spaw* expression (Fig. 4G). These data suggest that *lamb1a* deficiency in the KV alone only partially impairs L-R gene expression and that *lamb1a* also functions in other tissues, probably the notochord, to regulate L-R gene expression. Interestingly, *lamb1a* knockdown in the KV resulted in a significant increase of inverted liver and pancreas phenotype. However, complete inversion of liver and pancreas sidedness was never observed in *lamb1a*^{s804} mutants, despite bilateral expression of *spaw*. The differences between *lamb1a*^{s804} mutants and embryos with *lamb1a* knockdown in the KV thus suggested that dysregulation of L-R gene expression alone could not account for the gut-looping defects in the *lamb1a*^{s804} mutants.

Asymmetric migration of the LPM is impaired in *lamb1a*^{s804} mutants

We have previously shown that the leftward gut-looping morphogenesis results from the asymmetric migration of the LPM, and that LPM migration relies on the remodeling of laminin distribution in the basement membrane at the gut-LPM boundary (Horne-Badovinac et al., 2003; Yin et al., 2010). To analyze the dynamics of the LPM during gut looping in *lamb1a*^{s804} mutants, we tracked LPM migration in the gut looping region between 24 and 30 hpf, using the *Tg(hand2:EGFP)* line combined with phalloidin staining to visualize the LPM and adjacent tissues. At 25 hpf, the left and right LPM in both wild-type and *lamb1a*^{s804} mutant embryos have converged to the midline, dorsal to the gut endoderm and *Tg(hand2:EGFP)*-expressing cells in both wild types and mutants are organized in a single row of cells situated in the ventral region of the LPM (Fig. 5A,B). At 30 hpf, asymmetric morphogenetic movements result in the asymmetric configuration of the LPM in wild-type embryos, with the right LPM extending ventrally and across the left LPM (Fig. 5C,C′). In *lamb1a*^{s804} mutants, however, the left and right LPM remain dorsal to the gut, lacking asymmetry after converging to the midline. Moreover, the morphology and distribution of the *Tg(hand2:EGFP)*-expressing cells is abnormal in some mutants (Fig. 5D-G). Based on the migration pattern and morphology of LPM cells, we classified four types of LPM phenotypes. In class I, the LPM is composed of two rows of epithelial cells with the *Tg(hand2:EGFP)*-expressing cells located in the ventral half. The left and right LPM undergo asymmetric migration and the gut loops to the left (Fig. 5D). In class II, the majority of the LPM cells exhibit epithelial polarity, but there are more than two rows of cells in the left and right LPM. Moreover, the left and right LPM fail to undergo asymmetric migration, remaining dorsal to the gut (Fig. 5E). In class III, the LPM cells round up and the two-row organization of the LPM is also compromised (Fig. 5F). Last, in class IV, embryos exhibit aberrant intrusion of *Tg(hand2:EGFP)*-expressing cells into the gut, in addition to defects in epithelial morphology and LPM organization (Fig. 5G). In wild types, over 90% of the embryos exhibit the class I phenotype (n=10). Among the mutants examined here (n=24), 40% were class IV, 25% were class III and 15% were class II. Only 10% had normal asymmetric LPM migration and leftward gut-looping (Fig. 5H). In wild types, the left and right LPM are composed of equal numbers of *Tg(hand2:EGFP)*-expressing and non-expressing cells throughout the time course of gut-looping morphogenesis. Whereas *lamb1a*^{s804} mutants maintain equal numbers of *Tg(hand2:EGFP)*-expressing and non-expressing cells prior to gut looping (Fig. 5I), later there is an increased number of *Tg(hand2:EGFP)*-expressing cells at the expense of *Tg(hand2:EGFP)*-non-expressing cells (Fig. 5I), with the total number of LPM cells comparable with wild type (data not shown). The severe disorganization of *Tg(hand2:EGFP)*-expressing cells raised the possibility that their LPM cell identity might be compromised. Arguing against this possibility, the LPM markers *wnt2bb* (Fig. 5J) (Ober et al., 2006) and *bmp2b* (data not shown) (Chung et al., 2008) were expressed in the gut-looping region in *lamb1a*^{s804} mutants. Alternatively, complete loss of epithelial polarity also cannot explain the LPM phenotype in the mutants, as localized expression of the tight junction protein ZO-1 (Horne-Badovinac et al., 2001) (Fig. 5K) is still detected in the mutants, even though the mutant LPM is extremely disorganized and some cells protrude into the gut (Fig. 5K′).

Deficiency in L-R patterning alone cannot account for the LPM migration defects in *lamb1a*^{s804} mutants

We asked to what degree the disruption of L-R patterning due to impairment of the KV and notochord during somitogenesis was linked to the late LPM migration defects in *lamb1a*^{s804} mutants. A majority of *lamb1a*^{s804} mutants fail to undergo asymmetric LPM migration (Fig. 5H). Upon loss of *lamb1a* in the KV, however, the direction of LPM migration was randomized: 53% of the embryos showed normal asymmetric LPM migration (n=30), 33% showed reversed migration and 13% showed no asymmetric migration with both left and right LPM remaining dorsal to the gut (Fig. 6A-D,G). Therefore, Lamb1a deficiency in the KV is not solely responsible for the defective LPM morphogenesis in *lamb1a*^{s804} mutants.

We also examined other mutants that are deficient in notochord development. In *floating head/flh* and *no tail/ntl* mutants, specification and differentiation, respectively, of the notochord is defective (Schulte-Merker et al., 1994; Halpern et al., 1995; Talbot et al., 1995). As a consequence, these mutants show bilateral expression of L-R genes, similar to that observed in *lamb1a*^{s804} mutants (Bisgrove et al., 2000; Chin et al., 2000). We injected MO against *flh* or *ntl* at the one-cell stage. By 32 hpf, most control MO-injected embryos had undergone leftwards LPM migration, with only 2% showing no asymmetric migration (n=1/53). For the *flh* and *ntl* MO-injected embryos, 65% (n=32/49) and 51% (n=18/35), respectively, exhibited no asymmetric LPM migration, with both the left and right LPM remaining dorsal to the gut. Notably, LPM migration defects in *ntl*- and *flh*-deficient embryos were significantly less severe than those in *lamb1a*^{s804} mutants, where 80% fail to undergo asymmetric LPM migration. Interestingly, the LPM of embryos with *lamb1a* knockdown in the KV as well as in those with global knockdown of *flh* or *ntl* function failed to show impairment of epithelial morphology or LPM composition. In summary, disrupting L-R patterning alone yields less severe LPM migration defects than those observed in *lamb1a*^{s804} mutants.

DISCUSSION

Here, we report a zebrafish *lamb1a* mutant allele that displays previously uncharacterized defects in asymmetric positioning of the liver and pancreas. Lamb1a function is required in the KV and notochord for early establishment of embryonic L-R asymmetry. Interestingly, KV-specific knockdown of *lamb1a* expression results

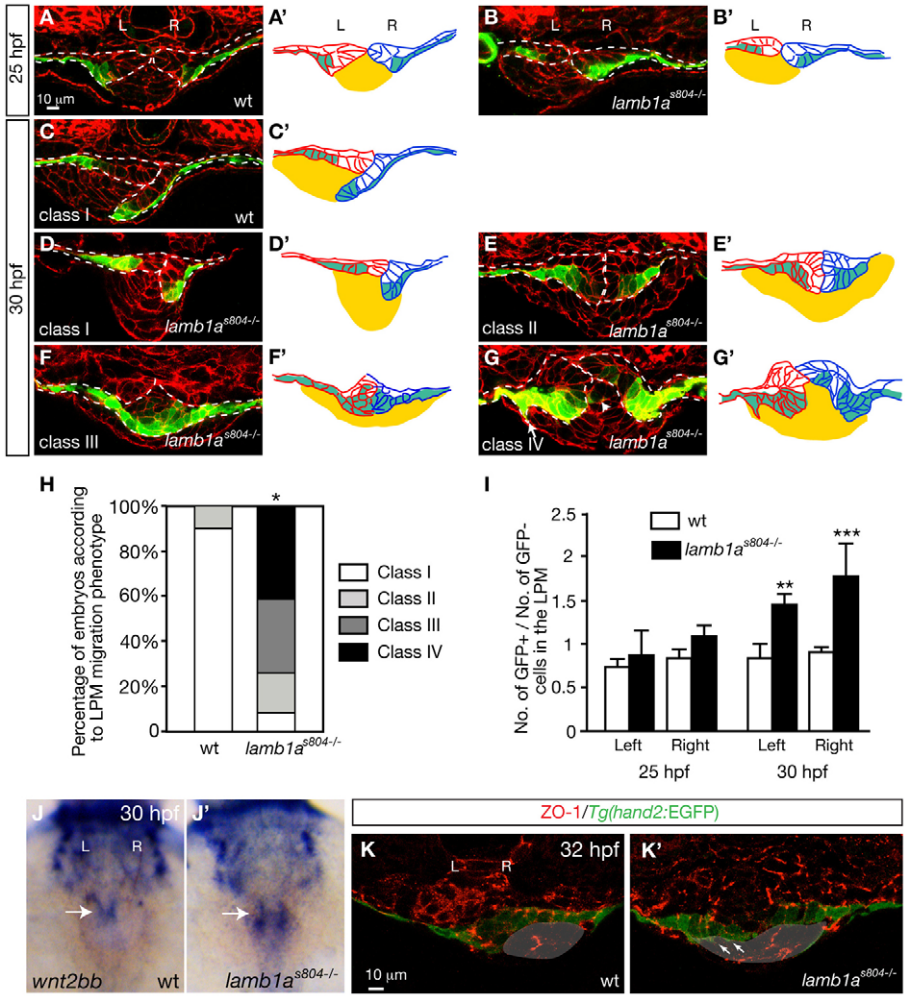

Fig. 5. Loss of Lamb1a function affects LPM morphogenesis essential for asymmetric LPM migration and gut looping. (**A**,**B**) Expression of *Tg(hand2:EGFP)* in the LPM of wild-type (*n*=5) and *lamb1a*^{s804} mutant (*n*=5) embryos at 25 hpf. GFP (green), phalloidin (red). (**C-G**) Four classes of LPM migration phenotypes were observed in wild-type (*n*=10) and *lamb1a*^{s804} mutant (*n*=24) embryos at 30 hpf. In G, the arrow indicates the aberrant protrusion of a *Tg(hand2:EGFP)*-expressing cell into the gut. The arrowhead indicates a *Tg(hand2:EGFP)*-expressing cell located inside the gut. (**A′-G′**) The LPM and gut shown in A-G. Gut (yellow); left LPM (red); right LPM (blue); *Tg(hand2:EGFP)*-expressing cells (green). (**H**) Proportions of wild-type (*n*=10) and *lamb1a*^{s804} mutant (*n*=24) embryos exhibiting the four classes of LPM migration phenotypes; *P<0.001. (**I**) Ratios (mean±s.e.m.) of *Tg(hand2:EGFP)*-expressing cells to *Tg(hand2:EGFP)*-non-expressing cells in the LPM at 25 and 30 hpf. Five wild-type and five mutants were examined at 25 hpf. Ten wild-type and 24 mutants were examined at 30 hpf. Asterisks indicate statistical significance: **P<0.05; ***P<0.01. (**J**,**J′**) Expression of the LPM marker *wnt2bb* in wild-type (J) and *lamb1a*^{s804} mutant (J′) embryos at 30 hpf. Arrows indicate the expression in the LPM at the gut-looping region. Dorsal views, anterior towards the top. (**K**,**K′**) Expression of the tight junction protein ZO-1 (red) and *Tg(hand2:EGFP)* (green) in the LPM of wild-type (K) and *lamb1a*^{s804} mutant (K′) embryos at 32 hpf. Arrows in K′ indicate LPM cells that protrude into the gut but still maintain localized ZO-1 expression. (A-G,K,K′) Transverse sections, dorsal towards the top. Scale bars: 10 μm. Broken lines outline the LPM. Shadows in K and K′ outline the gut primordium. L, left; R, right.

in typical randomization of embryonic L-R asymmetry, with phenotypes including inversion of LPM asymmetry and liver/pancreas position. By contrast, loss of laminin function in the basement membrane associated with the LPM disrupts its epithelial organization and impedes its asymmetric migration. Consequently, gut-looping morphogenesis fails to occur properly and the liver and pancreas remain symmetric.

Lamb1a controls cilia length in the KV

Establishment of L-R asymmetry is a progressive process. At early stages, a directional fluid flow generated by the beating of ciliated cells in the node in mice, or the KV in zebrafish, induces cells on the left side of the vesicle to activate asymmetric gene expression (Nonaka et al., 1998; Okada et al., 1999; Amack and Yost, 2004). Integrity of the KV and ciliary activity is necessary to generate this L-R asymmetry. ECM proteins have been implicated in morphogenesis of the organizer. Fibronectin participates in the development of embryonic L-R asymmetry, by controlling the organization of cells into a single layer in the mouse node, without affecting cilia length (Pulina et al., 2011). In zebrafish, integrin α5 is expressed in the dorsal forerunner cells and is required for the morphogenesis of a single intact KV (Ablooglu et al., 2010).

Our data show that Lamb1a controls cilia length in the KV. We identify a distinctive distribution of Lam1 that is associated with sites of cilia formation during KV morphogenesis. Interestingly, in mammals, Lam-511 regulates primary cilia formation during dermal papilla development (Gao et al., 2008), suggesting that the role of laminin in ciliogenesis may be conserved in different organs and

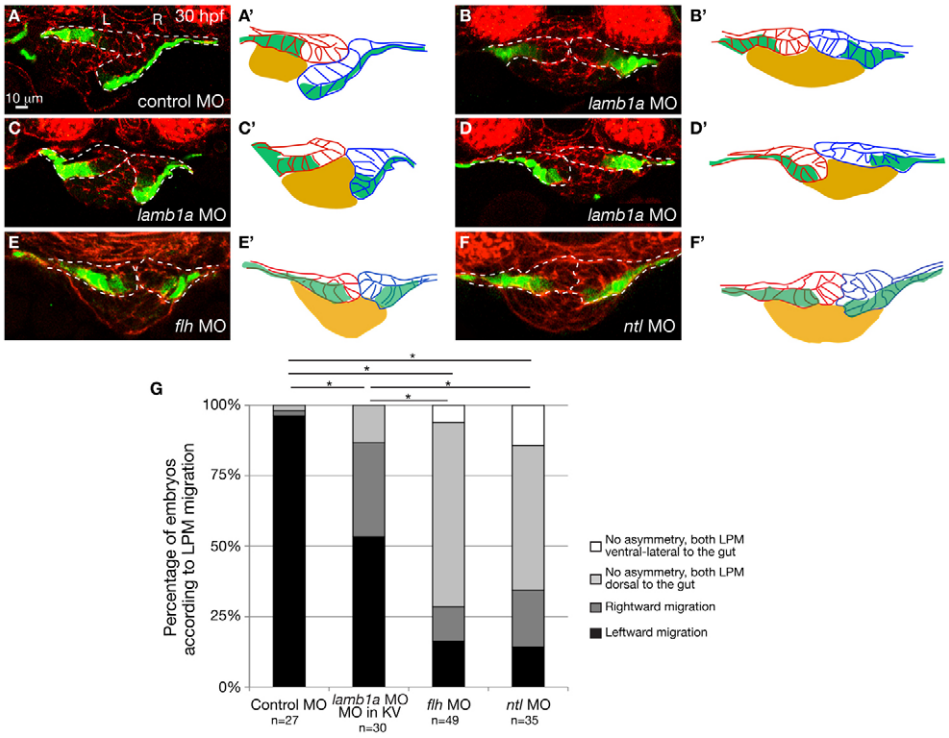

Fig. 6. *lamb1a* knock-down in the KV as well as global knock-down of *flh* and *ntl* randomized the direction of LPM migration without altering epithelial polarity or composition of the LPM. (**A-F**) Expression of *Tg(hand2:EGFP)* in the LPM of embryos injected with control (A) or *lamb1a* (B-D) MO into the KV at 3 hpf, or *flh* MO (E) or *ntl* MO (F) at the one-cell stage. Transverse sections, dorsal towards the top. Scale bar: 10 μm. Dashed lines outline the LPM. L, left; R, right. (**A′-F′**) The LPM and gut shown in A-D. Gut (yellow), left LPM (red), right LPM (blue), *Tg(hand2:EGFP)*-expressing cells (green). (**G**) Proportions of control, *lamb1a, flh and ntl* MO-injected embryos exhibiting different directions of LPM migration. Effect of *lamb1a* knockdown in the KV on LPM migration is statistically significant, when compared with control, *flh* and *ntl* morphants (*P<0.001). The distribution of LPM migration phenotype is similar in *flh* and *ntl* morphants (P=0.794), but significantly different in embryos injected with *lamb1a* MO in the KV or with the control MO.

across species. Yet the mechanism by which Lamb1a modulates cilia formation is not clear. Studies of primary cilia of chick chondroblasts indicate that the ECM directly signals to cells via integrins α2, α3 and β1, which anchor the cilium to collagen fibers within the ECM (Jensen et al., 2004; McGlashan et al., 2006). It is possible that Lamb1a is involved in establishing the cellular property of the ciliated cells essential for cilia formation.

Previous studies in zebrafish have identified signaling molecules that regulate KV cilia formation. For example, defects in cilia length associated with deficiency in FGF or Notch signaling pathways have been described to affect fluid flow in the KV, which consequently results in defects in L-R asymmetry (Albertson and Yelick, 2005; Neugebauer et al., 2009; Yamauchi et al., 2009; Lopes et al., 2010). Activation of Wnt/β-catenin signaling results in loss of cardiac asymmetry, and affects morphology of the KV, with larger KV and increased cilia number. By contrast, reduction of Wnt3 or Wnt8 results in shorter cilia and randomization of *spaw* expression, with effects on both heart and digestive organs sidedness (Nakaya et al., 2005; Lin and Xu, 2009; Caron et al., 2012). In addition, the Rho kinase Rock2b controls anterior-posterior asymmetric placement of ciliated cells in the KV, and subsequently L-R patterning of the embryo (Wang et al., 2011). In *lamb1a*^{s804} mutants, we observed that impaired cilia length and movements partially contribute to defects in L-R patterning, resulting in variable defects in the dynamics or directionality of the fluid flow in the KV. It is intriguing to speculate that Lamb1a and its integrin receptors might serve as mediators of the signaling pathways described above, to modulate cilia formation.

Regulation of notochord differentiation by Lamb1a is crucial for establishment of L-R gene expression

After initiation of left-sided signaling, the notochord generates a midline barrier that restricts the cascade of gene expression to the left side of the embryo (Lee and Anderson, 2008). Mutants defective in notochord formation often exhibit randomization of organ laterality (Danos and Yost, 1996). The notochord of *lamb1a*^{s804} mutants appears atrophic and collapsed, consistent with the role of laminins in the formation of this structure. In zebrafish, laminin subunits β1 and γ1 are essential for establishment of the peri-notochordal basement membrane and organization of the notochord sheath, which provides physical resistance against the pressure exerted by the inflated notochord vacuoles (Parsons et al., 2002). Importantly, differentiation of the notochord is also impaired in the *lamb1a* and *lamg1* mutants, suggesting that there may be signals emanating from the ECM in the basement membrane to regulate chordamesoderm differentiation (Stemple, 2005).

Analysis of *ntl* expression showed that the notochord defect in *lamb1a*^{s804} mutants does not distribute along its full extension, but rather is restricted to the liver and pancreas-forming region. Coincident with the intact *ntl* expression in the more anterior region of the notochord, heart sidedness was not affected in the *lamb1a*^{s804} mutants. The independent phenotypes of the heart and gut laterality in *lamb1a*^{s804} mutants suggest that heterotaxy of organ laterality caused by midline defects is dependent on distinct domains along the anteroposterior axis (Bisgrove et al., 2000; Chin et al., 2000). Moreover, our observation that fewer *ntl*- and *flh*-deficient embryos fail to undergo asymmetric LPM migration compared with *lamb1a*^{s804} mutants indicates that impairment in the notochord alone cannot account for the gut laterality defects seen in *lamb1a*^{s804} mutants.

Localized expression of Lam1 controls asymmetric migration of the LPM

Asymmetric migration of the left and right LPM is essential for leftward gut-looping morphogenesis (Horne-Badovinac et al., 2003). Lam1 is expressed in a dynamic pattern at the interface between the LPM and gut endoderm during LPM migration, and remodeling of the ECM has been associated with establishment of proper contacts between these tissues, which are necessary to drive

morphogenetic movements (Yin et al., 2010). *lamb1a*^{s804} mutants lack the coiled-coil domain of the β1 chain, and expression of Lam1 protein is detected as intracellular speckles, instead of the discrete continuous expression observed in the basement membranes of wild-type embryos. This observation is consistent with the model proposed for assembly and secretion of Lam1, in which secretion of the functional trimeric laminin requires a first step of intracellular dimerization of subunits β1 and γ1, followed by assembly with an α1 chain (Peters et al., 1985; Kammerer et al., 1995; Kumagai et al., 1997; Yurchenco et al., 1997; Goto et al., 2001; Urbano et al., 2009). In the absence of proper laminin deposition, the left and right LPM fail to undergo asymmetric migration, and remain aligned dorsal to the gut.

By tracking the LPM migration at cellular resolution, we uncovered distinctive phenotypes in the LPM of *lamb1a*^{s804} mutants that may account for the failure of LPM migration. Laminins have been implicated in the establishment of cell polarization in embryonic cells (Li et al., 2003). Establishment of epithelial polarity in the LPM is absolutely essential for asymmetric LPM migration and gut looping (Horne-Badovinac et al., 2003; Yin et al., 2010). Mutant LPM cells are correctly specified and the organization of the LPM is unaffected prior to LPM migration. However, as the LPM migrates to the midline, in majority of *lamb1a*^{s804} mutants the LPM failed to align into two rows of cells and its epithelial architecture is compromised. Interestingly, we detected localized expression of ZO-1 in mutant LPM cells, indicating that their epithelial polarity is not completely abolished. In the absence of laminin in the basement membrane, the mutant LPM cells may be partially depolarized and undergo epithelial-to-mesenchymal transition, contributing to the failure of LPM migration.

In addition to the defects in epithelial cell morphology, the composition of the LPM is impaired in *lamb1a*^{s804} mutants, as demonstrated by an increased number of *Tg(hand2:EGFP)*-expressing cells at the expense of the non-expressing cells. We also found that in some of *lamb1a*^{s804} mutants, the LPM cells aberrantly protruded into the gut. During gut-looping morphogenesis, the LPM cells coordinate with one another and migrate as a coherent sheet. In *lamb1a*^{s804} mutants, the lack of basement membrane at the LPM-gut boundary allows some LPM cells to escape from the LPM and protrude into the gut. Such cell behavior could disrupt the normal communication between the LPM cells and impede the collective migration of the LPM. An intriguing possibility is that the basement membrane may either sequester or mediate the migration cues secreted from the LPM or the gut endoderm. In *lamb1a*^{s804} mutants, such regulation of migration cues was absent due to the deficiency in the basement membrane. Supporting this notion, a recent report on L-R asymmetry in *Xenopus* showed that the ECM is a principal surface of Nodal and Lefty accumulation and that sulfated proteoglycans facilitate long distance movement of Nodal (Marjoram and Wright, 2011). Similarly, in *Drosophila* and mouse, ECM components have been implicated in facilitating transport of BMPs, FGF and Nodal (García-García and Anderson, 2003; Belenkaya et al., 2004; Oki et al., 2007).

Our results indicate that deficiency of Lamβ1 disrupts both the L-R patterning during somitogenesis and the asymmetric LPM migration during later development. KV-specific knock-down of *lamb1a* randomized L-R patterning and the directionality of LPM migration. However, it did not impair epithelial polarity or composition of the LPM. Despite these observations, early and late roles of Lamb1a in organ laterality cannot be completely uncoupled. Unlike embryos with Lamb1a deficiency in the KV, *lamb1a*^{s804} mutants show bilateral expression of *spaw* in the LPM during somitogenesis. Whether such aberrant expression of *spaw* has any impact on LPM polarity and composition is not yet clear.

Lamb1a is necessary for organization of pancreas and liver architecture

In addition to defects in L-R organ asymmetry, the architecture of the liver and pancreas is also affected in *lamb1a*^{s804} mutants. Diminished expression of laminin affects the adhesion of hepatic and pancreatic cells, as well as the integrity of other endodermal-derived tissues. This phenotype is consistent with a crucial role for basement membranes in mediating cell adhesion and tissue organization (Li et al., 2003). Moreover, in the mutant pancreas an increased number of endocrine cells are associated with the hepatopancreatic duct, suggesting that the lack of laminin might affect the homing of newly differentiated endocrine cells. Laminins and cell surface-associated ECM proteins of the basement membranes are essential for the survival and in vitro function of pancreatic islets and liver cells (Stamatoglou and Hughes, 1994; Nagaki et al., 1995; Paraskevas et al., 2000; Schroeder et al., 2006); however, their role in organogenesis is not clear. Understanding their normal function in development and their link to signaling pathways is crucial for their future use in a therapeutic context.

Acknowledgements

We thank Elke Ober, Holly Field, Heather Verkade and other members of the ENU screen team, as well as Chantilly (Munson) Apollon for sharing reagents and expertise in LR organ asymmetry. We thank Mike Parsons for the *grumpy* allele and Thai Truong for assistance with settings for live imaging of the KV flow. Thanks to Zhaoxia Sun for sharing before publication her protocol for the analysis of KV flow, and to Pablo Oteíza and Hiroaki Ishikawa for advice.

Funding

T.H.-H. was supported by a Pew Latin American Fellowship in the Biomedical Sciences and by a California Institute for Regenerative Medicine Training Grant [T2-00006]. C.Y. is supported by an National Institutes of Health (NIH) K99 Award [AA020514], a University of California at San Francisco Liver Center Pilot/Feasibility Award [NIH P30DK026743] and the Cincinnati Children's Hospital Research Foundation. This work was supported in part by grants from the NIH [P50 HG004071 to M.E.B., R01DK060322 to D.Y.R.S.] and from the Packard Foundation (to D.Y.R.S.). Deposited in PMC for release after 12 months.

Author contributions

T.H.-H. and C.Y. designed and performed experiments, analyzed data and wrote the manuscript. D.E.S.K. performed experiments, analyzed data and edited the manuscript. M.E.B. and D.Y.R.S. supervised the work, including helping with experimental design, data, analysis and manuscript preparation.

References

Ablooglu, A. J., Tkachenko, E., Kang, J. and Shattil, S. J. (2010). Integrin alphaV is necessary for gastrulation movements that regulate vertebrate body asymmetry. *Development* **137**, 3449-3458.

Albertson, R. C. and Yelick, P. C. (2005). Roles for fgf8 signaling in left-right patterning of the visceral organs and craniofacial skeleton. *Dev. Biol.* **283**, 310-321.

Alexander, J. and Stainier, D. Y. (1999). A molecular pathway leading to endoderm formation in zebrafish. *Curr. Biol.* **9**, 1147-1157.

Amack, J. D. and Yost, H. J. (2004). The T box transcription factor no tail in ciliated cells controls zebrafish left-right asymmetry. *Curr. Biol.* **14**, 685-690.

Argenton, F., Zecchin, E. and Bortolussi, M. (1999). Early appearance of pancreatic hormone-expressing cells in the zebrafish embryo. *Mech. Dev.* **87**, 217-221.

Beck, K., Hunter, I. and Engel, J. (1990). Structure and function of laminin: anatomy of a multidomain glycoprotein. *FASEB J.* **4**, 148-160.

Belenkaya, T. Y., Han, C., Yan, D., Opoka, R. J., Khodoun, M., Liu, H. and Lin, X. (2004). Drosophila Dpp morphogen movement is independent of dynamin-mediated endocytosis but regulated by the glypican members of heparan sulfate proteoglycans. *Cell* **119**, 231-244.

Biemar, F., Argenton, F., Schmidtke, R., Epperlein, S., Peers, B. and Driever, W. (2001). Pancreas development in zebrafish: early dispersed appearance of endocrine hormone expressing cells and their convergence to form the definitive islet. *Dev. Biol.* **230**, 189-203.

Bisgrove, B. W., Essner, J. J. and Yost, H. J. (1999). Regulation of midline development by antagonism of lefty and nodal signaling. *Development* **126**, 3253-3262.
Bisgrove, B. W., Essner, J. J. and Yost, H. J. (2000). Multiple pathways in the midline regulate concordant brain, heart and gut left-right asymmetry. *Development* **127**, 3567-3579.
Branford, W. W., Essner, J. J. and Yost, H. J. (2000). Regulation of gut and heart left-right asymmetry by context-dependent interactions between xenopus lefty and BMP4 signaling. *Dev. Biol.* **223**, 291-306.
Campione, M., Steinbeisser, H., Schweickert, A., Deissler, K., van Bebber, F., Lowe, L. A., Nowotschin, S., Viebahn, C., Haffter, P., Kuehn, M. R. et al. (1999). The homeobox gene Pitx2: mediator of asymmetric left-right signaling in vertebrate heart and gut looping. *Development* **126**, 1225-1234.
Capdevila, J., Vogan, K. J., Tabin, C. J. and Izpisúa Belmonte, J. C. (2000). Mechanisms of left-right determination in vertebrates. *Cell* **101**, 9-21.
Caron, A., Xu, X. and Lin, X. (2012). Wnt/β-catenin signaling directly regulates Foxj1 expression and ciliogenesis in zebrafish Kupffer's vesicle. *Development* **139**, 514-524.
Chen, J. N., van Bebber, F., Goldstein, A. M., Serluca, F. C., Jackson, D., Childs, S., Serbedzija, G., Warren, K. S., Mably, J. D., Lindahl, P. et al. (2001). Genetic steps to organ laterality in zebrafish. *Comp. Funct. Genomics* **2**, 60-68.
Chin, A. J., Tsang, M. and Weinberg, E. S. (2000). Heart and gut chiralities are controlled independently from initial heart position in the developing zebrafish. *Dev. Biol.* **227**, 403-421.
Chung, W. S., Shin, C. H. and Stainier, D. Y. (2008). Bmp2 signaling regulates the hepatic versus pancreatic fate decision. *Dev. Cell* **15**, 738-748.
Clanton, J. A., Hope, K. D. and Gamse, J. T. (2013). Fgf signaling governs cell fate in the zebrafish pineal complex. *Development* **140**, 323-332.
Collignon, J., Varlet, I. and Robertson, E. J. (1996). Relationship between asymmetric nodal expression and the direction of embryonic turning. *Nature* **381**, 155-158.
Danos, M. C. and Yost, H. J. (1996). Role of notochord in specification of cardiac left-right orientation in zebrafish and Xenopus. *Dev. Biol.* **177**, 96-103.
Davis, N. M., Kurpios, N. A., Sun, X., Gros, J., Martin, J. F. and Tabin, C. J. (2008). The chirality of gut rotation derives from left-right asymmetric changes in the architecture of the dorsal mesentery. *Dev. Cell* **15**, 134-145.
Engel, J., Odermatt, E., Engel, A., Madri, J. A., Furthmayr, H., Rohde, H. and Timpl, R. (1981). Shapes, domain organizations and flexibility of laminin and fibronectin, two multifunctional proteins of the extracellular matrix. *J. Mol. Biol.* **150**, 97-120.
Essner, J. J., Branford, W. W., Zhang, J. and Yost, H. J. (2000). Mesendoderm and left-right brain, heart and gut development are differentially regulated by pitx2 isoforms. *Development* **127**, 1081-1093.
Essner, J. J., Amack, J. D., Nyholm, M. K., Harris, E. B. and Yost, H. J. (2005). Kupffer's vesicle is a ciliated organ of asymmetry in the zebrafish embryo that initiates left-right development of the brain, heart and gut. *Development* **132**, 1247-1260.
Field, H. A., Ober, E. A., Roeser, T. and Stainier, D. Y. (2003). Formation of the digestive system in zebrafish. I. Liver morphogenesis. *Dev. Biol.* **253**, 279-290.
Gao, J., DeRouen, M. C., Chen, C. H., Nguyen, M., Nguyen, N. T., Ido, H., Harada, K., Sekiguchi, K., Morgan, B. A., Miner, J. H. et al. (2008). Laminin-511 is an epithelial message promoting dermal papilla development and function during early hair morphogenesis. *Genes Dev.* **22**, 2111-2124.
García-García, M. J. and Anderson, K. V. (2003). Essential role of glycosaminoglycans in Fgf signaling during mouse gastrulation. *Cell* **114**, 727-737.
Goto, A., Aoki, M., Ichihara, S. and Kitagawa, Y. (2001). alpha-, beta- or gamma-chain-specific RNA interference of laminin assembly in Drosophila Kc167 cells. *Biochem. J.* **360**, 167-172.
Halpern, M. E., Ho, R. K., Walker, C. and Kimmel, C. B. (1993). Induction of muscle pioneers and floor plate is distinguished by the zebrafish no tail mutation. *Cell* **75**, 99-111.
Halpern, M. E., Thisse, C., Ho, R. K., Thisse, B., Riggleman, B., Trevarrow, B., Weinberg, E. S., Postlethwait, J. H. and Kimmel, C. B. (1995). Cell-autonomous shift from axial to paraxial mesodermal development in zebrafish floating head mutants. *Development* **121**, 4257-4264.
Hecksher-Sørensen, J., Watson, R. P., Lettice, L. A., Serup, P., Eley, L., De Angelis, C., Ahlgren, U. and Hill, R. E. (2004). The splanchnic mesodermal plate directs spleen and pancreatic laterality, and is regulated by Bapx1/Nkx3.2. *Development* **131**, 4665-4675.
Ho, C. Y., Houart, C., Wilson, S. W. and Stainier, D. Y. (1999). A role for the extraembryonic yolk syncytial layer in patterning the zebrafish embryo suggested by properties of the hex gene. *Curr. Biol.* **9**, 1131-1134.
Horne-Badovinac, S., Lin, D., Waldron, S., Schwarz, M., Mbamalu, G., Pawson, T., Jan, Y., Stainier, D. Y. and Abdelilah-Seyfried, S. (2001). Positional cloning of heart and soul reveals multiple roles for PKC lambda in zebrafish organogenesis. *Curr. Biol.* **11**, 1492-1502.
Horne-Badovinac, S., Rebagliati, M. and Stainier, D. Y. (2003). A cellular framework for gut-looping morphogenesis in zebrafish. *Science* **302**, 662-665.
Jensen, C. G., Poole, C. A., McGlashan, S. R., Marko, M., Issa, Z. I., Vujcich, K. V. and Bowser, S. S. (2004). Ultrastructural, tomographic and confocal imaging of the chondrocyte primary cilium in situ. *Cell Biol. Int.* **28**, 101-110.
Kammerer, R. A., Antonsson, P., Schulthess, T., Fauser, C. and Engel, J. (1995). Selective chain recognition in the C-terminal α-helical coiled-coil region of laminin. *J. Mol. Biol.* **250**, 64-73.
Kikuchi, K., Holdway, J. E., Major, R. J., Blum, N., Dahn, R. D., Begemann, G. and Poss, K. D. (2011). Retinoic acid production by endocardium and epicardium is an injury response essential for zebrafish heart regeneration. *Dev. Cell* **20**, 397-404.
Kumagai, C., Kadowaki, T. and Kitagawa, Y. (1997). Disulfide-bonding between Drosophila laminin beta and gamma chains is essential for alpha chain to form alpha betagamma trimer. *FEBS Lett.* **412**, 211-216.
Kurpios, N. A., Ibañes, M., Davis, N. M., Lui, W., Katz, T., Martin, J. F., Izpisúa Belmonte, J. C. and Tabin, C. J. (2008). The direction of gut looping is established by changes in the extracellular matrix and in cell:cell adhesion. *Proc. Natl. Acad. Sci. USA* **105**, 8499-8506.
Latimer, A. and Jessen, J. R. (2010). Extracellular matrix assembly and organization during zebrafish gastrulation. *Matrix Biology* **29**, 89-96.
Lee, J. D. and Anderson, K. V. (2008). Morphogenesis of the node and notochord: the cellular basis for the establishment and maintenance of left-right asymmetry in the mouse. *Dev. Dyn.* **237**, 3464-3476.
Levin, M. (2005). Left-right asymmetry in embryonic development: a comprehensive review. *Mech. Dev.* **122**, 3-25.
Levin, M., Johnson, R. L., Stern, C. D., Kuehn, M. and Tabin, C. (1995). A molecular pathway determining left-right asymmetry in chick embryogenesis. *Cell* **82**, 803-814.
Li, S., Edgar, D., Fässler, R., Wadsworth, W. and Yurchenco, P. D. (2003). The role of laminin in embryonic cell polarization and tissue organization. *Dev. Cell* **4**, 613-624.
Lin, X. and Xu, X. (2009). Distinct functions of Wnt/beta-catenin signaling in KV development and cardiac asymmetry. *Development* **136**, 207-217.
Logan, M., Pagán-Westphal, S. M., Smith, D. M., Paganessi, L. and Tabin, C. J. (1998). The transcription factor Pitx2 mediates situs-specific morphogenesis in response to left-right asymmetric signals. *Cell* **94**, 307-317.
Long, S., Ahmad, N. and Rebagliati, M. (2003). The zebrafish nodal-related gene southpaw is required for visceral and diencephalic left-right asymmetry. *Development* **130**, 2303-2316.
Lopes, S. S., Lourenço, R., Pacheco, L., Moreno, N., Kreiling, J. and Saúde, L. (2010). Notch signalling regulates left-right asymmetry through ciliary length control. *Development* **137**, 3625-3632.
Lowe, L. A., Supp, D. M., Sampath, K., Yokoyama, T., Wright, C. V., Potter, S. S., Overbeek, P. and Kuehn, M. R. (1996). Conserved left-right asymmetry of nodal expression and alterations in murine situs inversus. *Nature* **381**, 158-161.
Lustig, K. D., Kroll, K., Sun, E., Ramos, R., Elmendorf, H. and Kirschner, M. W. (1996). A Xenopus nodal-related gene that acts in synergy with noggin to induce complete secondary axis and notochord formation. *Development* **122**, 3275-3282.
Marjoram, L. and Wright, C. (2011). Rapid differential transport of Nodal and Lefty on sulfated proteoglycan-rich extracellular matrix regulates left-right asymmetry in Xenopus. *Development* **138**, 475-485.
McGlashan, S. R., Jensen, C. G. and Poole, C. A. (2006). Localization of extracellular matrix receptors on the chondrocyte primary cilium. *J. Histochem. Cytochem* **54**, 1005-1014.
Meno, C., Saijoh, Y., Fujii, H., Ikeda, M., Yokoyama, T., Yokoyama, M., Toyoda, Y. and Hamada, H. (1996). Left-right asymmetric expression of the TGF beta-family member lefty in mouse embryos. *Nature* **381**, 151-155.
Meno, C., Shimono, A., Saijoh, Y., Yashiro, K., Mochida, K., Ohishi, S., Noji, S., Kondoh, H. and Hamada, H. (1998). lefty-1 is required for left-right determination as a regulator of lefty-2 and nodal. *Cell* **94**, 287-297.
Miner, J. H. (2008). Laminins and their roles in mammals. *Microsc. Res. Tech.* **71**, 349-356.
Nagaki, M., Shidoji, Y., Yamada, Y., Sugiyama, A., Tanaka, M., Akaike, T., Ohnishi, H., Moriwaki, H. and Muto, Y. (1995). Regulation of hepatic genes and liver transcription factors in rat hepatocytes by extracellular matrix. *Biochem. Biophys. Res. Commun.* **210**, 38-43.
Nakamura, T., Mine, N., Nakaguchi, E., Mochizuki, A., Yamamoto, M., Yashiro, K., Meno, C. and Hamada, H. (2006). Generation of robust left-right asymmetry in the mouse embryo requires a self-enhancement and lateral-inhibition system. *Dev. Cell* **11**, 495-504.
Nakaya, M. A., Biris, K., Tsukiyama, T., Jaime, S., Rawls, J. A. and Yamaguchi, T. P. (2005). Wnt3a links left-right determination with segmentation and anteroposterior axis elongation. *Development* **132**, 5425-5436.
Nasevicius, A. and Ekker, S. C. (2000). Effective targeted gene 'knockdown' in zebrafish. *Nat. Genet.* **26**, 216-220.
Neugebauer, J. M., Amack, J. D., Peterson, A. G., Bisgrove, B. W. and Yost, H. J. (2009). FGF signalling during embryo development regulates cilia length in diverse epithelia. *Nature* **458**, 651-654.

Nonaka, S., Tanaka, Y., Okada, Y., Takeda, S., Harada, A., Kanai, Y., Kido, M. and Hirokawa, N. (1998). Randomization of left-right asymmetry due to loss of nodal cilia generating leftward flow of extraembryonic fluid in mice lacking KIF3B motor protein. *Cell* **95**, 829-837.
Ober, E. A., Field, H. A. and Stainier, D. Y. (2003). From endoderm formation to liver and pancreas development in zebrafish. *Mech. Dev.* **120**, 5-18.
Ober, E. A., Verkade, H., Field, H. A. and Stainier, D. Y. (2006). Mesodermal Wnt2b signalling positively regulates liver specification. *Nature* **442**, 688-691.
Okada, Y., Nonaka, S., Tanaka, Y., Saijoh, Y., Hamada, H. and Hirokawa, N. (1999). Abnormal nodal flow precedes situs inversus in iv and inv mice. *Mol. Cell* **4**, 459-468.
Oki, S., Hashimoto, R., Okui, Y., Shen, M. M., Mekada, E., Otani, H., Saijoh, Y. and Hamada, H. (2007). Sulfated glycosaminoglycans are necessary for Nodal signal transmission from the node to the left lateral plate in the mouse embryo. *Development* **134**, 3893-3904.
Oteíza, P., Köppen, M., Concha, M. L. and Heisenberg, C. P. (2008). Origin and shaping of the laterality organ in zebrafish. *Development* **135**, 2807-2813.
Paraskevas, S., Maysinger, D., Wang, R., Duguid, T. P. and Rosenberg, L. (2000). Cell loss in isolated human islets occurs by apoptosis. *Pancreas* **20**, 270-276.
Parsons, M. J., Pollard, S. M., Saúde, L., Feldman, B., Coutinho, P., Hirst, E. M. and Stemple, D. L. (2002). Zebrafish mutants identify an essential role for laminins in notochord formation. *Development* **129**, 3137-3146.
Peters, B. P., Hartle, R. J., Krzesicki, R. F., Kroll, T. G., Perini, F., Balun, J. E., Goldstein, I. J. and Ruddon, R. W. (1985). The biosynthesis, processing, and secretion of laminin by human choriocarcinoma cells. *J. Biol. Chem.* **260**, 14732-14742.
Piedra, M. E., Icardo, J. M., Albajar, M., Rodriguez-Rey, J. C. and Ros, M. A. (1998). Pitx2 participates in the late phase of the pathway controlling left-right asymmetry. *Cell* **94**, 319-324.
Piperno, G. and Fuller, M. T. (1985). Monoclonal antibodies specific for an acetylated form of alpha-tubulin recognize the antigen in cilia and flagella from a variety of organisms. *J. Cell Biol.* **101**, 2085-2094.
Pulina, M. V., Hou, S. Y., Mittal, A., Julich, D., Whittaker, C. A., Holley, S. A., Hynes, R. O. and Astrof, S. (2011). Essential roles of fibronectin in the development of the left-right embryonic body plan. *Dev. Biol.* **354**, 208-220.
Ryan, A. K., Blumberg, B., Rodriguez-Esteban, C., Yonei-Tamura, S., Tamura, K., Tsukui, T., de la Peña, J., Sabbagh, W., Greenwald, J., Choe, S. et al. (1998). Pitx2 determines left-right asymmetry of internal organs in vertebrates. *Nature* **394**, 545-551.
Schroeder, I. S., Rolletschek, A., Blyszczuk, P., Kania, G. and Wobus, A. M. (2006). Differentiation of mouse embryonic stem cells to insulin-producing cells. *Nat. Protoc.* **1**, 495-507.
Schulte-Merker, S., Ho, R. K., Herrmann, B. G. and Nüsslein-Volhard, C. (1992). The protein product of the zebrafish homologue of the mouse T gene is expressed in nuclei of the germ ring and the notochord of the early embryo. *Development* **116**, 1021-1032.
Schulte-Merker, S., van Eeden, F. J., Halpern, M. E., Kimmel, C. B. and Nüsslein-Volhard, C. (1994). no tail (ntl) is the zebrafish homologue of the mouse T (Brachyury) gene. *Development* **120**, 1009-1015.
Stainier, D. Y. (2002). A glimpse into the molecular entrails of endoderm formation. *Genes Dev.* **16**, 893-907.
Stamatoglou, S. C. and Hughes, R. C. (1994). Cell adhesion molecules in liver function and pattern formation. *FASEB J.* **8**, 420-427.
Stemple, D. L. (2005). Structure and function of the notochord: an essential organ for chordate development. *Development* **132**, 2503-2512.
Tabin, C. J. (2006). The key to left-right asymmetry. *Cell* **127**, 27-32.
Talbot, W. S., Trevarrow, B., Halpern, M. E., Melby, A. E., Farr, G., Postlethwait, J. H., Jowett, T., Kimmel, C. B. and Kimelman, D. (1995). A homeobox gene essential for zebrafish notochord development. *Nature* **378**, 150-157.
Thisse, C., Thisse, B., Schilling, T. F. and Postlethwait, J. H. (1993). Structure of the zebrafish snail1 gene and its expression in wild-type, spadetail and no tail mutant embryos. *Development* **119**, 1203-1215.
Trinh, L. A. and Stainier, D. Y. (2004). Fibronectin regulates epithelial organization during myocardial migration in zebrafish. *Dev. Cell* **6**, 371-382.
Urbano, J. M., Torgler, C. N., Molnar, C., Tepass, U., López-Varea, A., Brown, N. H., de Celis, J. F. and Martín-Bermudo, M. D. (2009). Drosophila laminins act as key regulators of basement membrane assembly and morphogenesis. *Development* **136**, 4165-4176.
Wang, G., Cadwallader, A. B., Jang, D. S., Tsang, M., Yost, H. J. and Amack, J. D. (2011). The Rho kinase Rock2b establishes anteroposterior asymmetry of the ciliated Kupffer's vesicle in zebrafish. *Development* **138**, 45-54.
Westerfield, M. (1995). *The Zebrafish Book: A Guide for the Laboratory Use of Zebrafish (Brachydanio rerio)*. Eugene, OR: University of Oregon Press.
Yamauchi, H., Miyakawa, N., Miyake, A. and Itoh, N. (2009). Fgf4 is required for left-right patterning of visceral organs in zebrafish. *Dev. Biol.* **332**, 177-185.
Yelon, D., Horne, S. A. and Stainier, D. Y. (1999). Restricted expression of cardiac myosin genes reveals regulated aspects of heart tube assembly in zebrafish. *Dev. Biol.* **214**, 23-37.
Yin, C., Kikuchi, K., Hochgreb, T., Poss, K. D. and Stainier, D. Y. (2010). Hand2 regulates extracellular matrix remodeling essential for gut-looping morphogenesis in zebrafish. *Dev. Cell* **18**, 973-984.
Yoshioka, H., Meno, C., Koshiba, K., Sugihara, M., Itoh, H., Ishimaru, Y., Inoue, T., Ohuchi, H., Semina, E. V., Murray, J. C. et al. (1998). Pitx2, a bicoid-type homeobox gene, is involved in a lefty-signaling pathway in determination of left-right asymmetry. *Cell* **94**, 299-305.
Yuan, S., Zhao, L. and Sun, Z. (2013). Dissecting the Functional Interplay Between the TOR Pathway and the Cilium in Zebrafish. *Methods Enzymol.* **525**, 159-189.
Yurchenco, P. D., Quan, Y., Colognato, H., Mathus, T., Harrison, D., Yamada, Y. and O'Rear, J. J. (1997). The alpha chain of laminin-1 is independently secreted and drives secretion of its beta- and gamma-chain partners. *Proc. Natl. Acad. Sci. USA* **94**, 10189-10194.